# Recursive decomposition of electromyographic signals with a varying number of active sources: Bayesian modelling and filtering

Tianyi Yu, Konstantin Akhmadeev, Éric Le Carpentier, Yannick Aoustin, Raphaël Gross, Yann Péréon, Dario Farina

# Recursive decomposition of electromyographic signals with a varying number of active sources: Bayesian modelling and filtering

Tianyi Yu, Konstantin Akhmadeev, Eric Le Carpentier, Yannick Aoustin, Raphaël Gross, Yann Péréon, Dario Farina, *Fellow, IEEE*

***Abstract*—This paper describes a sequential decomposition algorithm for single channel intramuscular electromyography (iEMG) generated by a varying number of active motor neurons. As in previous work, we establish a Hidden Markov Model of iEMG, in which each motor neuron spike train is modeled as a renewal process with inter-spike intervals following a discrete Weibull law and motor unit action potentials are modeled as impulse responses of linear time-invariant systems with known prior. We then expand this model by introducing an activation vector associated to the state vector of the Hidden Markov Model. This activation vector represents recruitment/derecruitment of motor units and is estimated together with the state vector using Bayesian filtering. Non-stationarity of the model parameters is addressed by means of a sliding window approach, thus making the algorithm adaptive to variations in contraction force and motor unit action potential waveforms. The algorithm was validated using simulated and experimental iEMG signals with varying number of active motor units. The experimental signals were acquired from the tibialis anterior and abductor digiti minimi muscles by fine wire and needle electrodes. The decomposition accuracy in both simulated and experimental signals exceeded 90% and the recruitment/derecruitment was successfully tracked by the algorithm. Because of its parallel structure, this algorithm can be efficiently accelerated, which lays the basis for its future real-time applications in human-machine interfaces, e.g. for prosthetic control.**

***Index Terms*—Biomedical signal processing, Hidden Markov models, Bayes methods, Recursive estimation, Deconvolution, Electromyography.**

TABLE I: Main notations

| | |
|---|---|
| $Y$ | iEMG signal |
| $\Omega$ | Set of indexes of all MUs |
| $A$ | Set of indexes of active MUs |
| $U$ | Spike trains |
| $W$ | White noise |
| $H$ | Vector of MU action potentials shapes |
| $\ell_{\text{IR}}$ | Maximum MUAPs length |
| $T$ | Sawtooth sequences |
| $S$ | Activation scenario |
| $\Theta = [t_0, \beta]$ | Vector containing the discrete Weibull distribution parameters: the location parameter and the concentration parameter |
| $t_{\text{R}}$ | Shifting parameter of discrete Weibull distribution, that is the refractory period |
| $\mathsf{Pr}$ | Probability |
| w.p. | with probability |
| $Y[n]$ | iEMG signal at time index $n$ |
| $Y^n$ | Vector containing the signal from time index 1 to $n$ |
| $\|n$ | Given $Y^n$ |
| $\mathsf{Pr}(T[n] = t[n])$ | Probability of the sawtooth sequences at time index $n$ being equal to a value $t[n]$. For all elements of the state vector, the uppercase symbols denote random variables, while the lowercase ones stand for their values. |

## I. Introduction

ELECTROMYOGRAPHIC (EMG) signal is the electrical activity of skeletal muscle fibers during a muscle contraction. This activity is driven by the motor neurons (MN) in the spinal cord that stimulate the muscle fibers by means of axonal action potential trains. The identification of individual MN discharge timings from EMG is termed EMG decomposition [1] and provides valuable information about the neural drive to the muscle. EMG decomposition jointly estimates motor unit action potential (MUAP) waveforms and spike train statistics, such as discharge rate. This information can be applied for the diagnosis of neuromuscular disorders [2], [3], [4], analysis of the muscle architecture [5], investigation of central strategies for motor control [6], [7] as well as for creating human-machine interfaces [8], [9], [10].

EMG signals are recorded using either surface (surface EMG, sEMG) or intramuscular electrodes (intramuscular EMG, iEMG). Intramuscular electrodes are more spatially selective [11] than surface ones so that an iEMG signal is usually produced by a limited number of MUs, with MUAPs distinct from the noise, although superimposed with each other in time.

The procedures for iEMG signal decomposition have been progressively improved from methods strongly based on the manual intervention of an operator [12], [13], [14] to fully automatic methods [9], [15], [16], [17], [18], [19], [20], [21], [22]. Nevertheless, some limitations remain. Most iEMG signal decomposition algorithms are based on MUAPs detection and clustering. Some of these do not take the temporal superimposition of MUAP waveforms into account [18], [19], leading to underestimation of the discharge rates, especially at higher contraction forces, when most of the MUAPs are

Manuscript created October 30, 2018; revised March 5, 2019.

This work was supported by the China Scholarship Council [grant number 201404490033] and by the University of Nantes as a part of project "Moderato".

Tianyi Yu, Konstantin Akhmadeev, Eric Le Carpentier and Yannick Aoustin are with the laboratory of digital sciences of Nantes, France. Raphaël Gross and Yann Péréon are with the hospital center of Nantes University, France. Dario Farina is with Imperial College London, England(correspondence e-mail: d.farina@imperial.ac.uk).

superimposed. Other algorithms (e.g., [15], [16], [17]) achieve complete decomposition in an off-line manner by first identifying and clustering the non-overlapped MUAPs and then iteratively searching for their occurrences in the superpositions. More recently, blind source separation approaches have been proposed to decompose multi-channel EMG signals [9], [20], [21] but their performance strongly depends on the number of available channels [22].

We have previously proposed a fully automatic single-channel iEMG decomposition algorithm that solves superimposed action potentials [23]. However, a major limitation of this previous algorithm is the constraint of a constant number of active motor units over time, thus effectively considering the signal stationary. This assumption causes the algorithm to diverge during periods of derecruitment of MNs. This constraint is substantial when considering practical applications since the cases of a constant number of active MNs for the full duration of the recording are limited.

In this paper, we propose a fundamental revision in the model used to derive the full decomposition by introducing the possibility of recruitment/derecruitment of MNs at any interval of time. This revision of the model introduces additional variables to be estimated and substantial changes in all parts of the previously proposed algorithm [23], thus effectively leading to a new method for decomposition of single-channel iEMG signals in unconstraint conditions. In this paper, we present a complete mathematical formulation of this new algorithm. This includes some elements from our previous work [23] that it is necessary to report again here for consistency in the mathematical derivations.

The algorithm is based on a Markov model of the iEMG, which takes into account the varying number of active MUs and the regularity of their spike trains (Part II). Joint superposition resolution, MUAPs shape updates and firing statistics estimation are achieved by applying the Bayes filtering (Part III). Simulated and experimental iEMG signals used to assess the proposed approach are described in Part IV. Their decomposition results are presented in Part IV. Limitations of the method, conclusions and perspectives are presented in Part VI. The proposed algorithm decomposes an iEMG in a sequential manner and thus lays the foundation for a real-time iEMG decomposition that can be applied to human-machine interfaces.

## II. Hidden Markov model of EMG signal

### A. From the physiology to a model structure

A motor unit (MU) is the elementary entity of the motor system. It consists of a MN located in the spinal cord and of a set of muscle fibers it innervates. Muscle contraction is achieved by concurrent activation of multiple MUs at a time. Its intensity is determined by the number of activated MUs, their sizes and their firing rates [24].

The sequences of actions potentials discharged by a MN are usually referred to as *spike trains*. Intervals between spikes are subject to physiological constrains. First, a sequence of inter-spike intervals (ISI) exhibit regular, rhythmic pattern, especially during static contractions. Second, inter-spike intervals

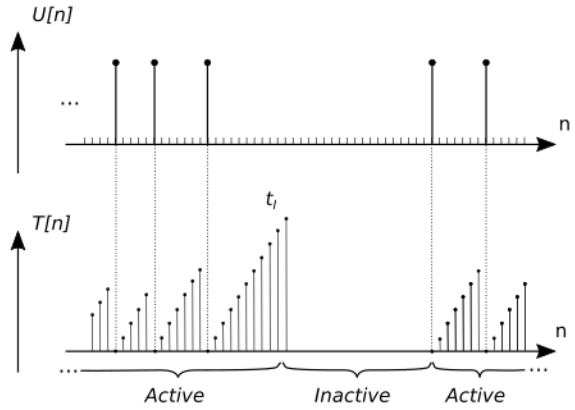


Fig. 1: Illustration of the relationship between the spike train $U[n]$ and corresponding sawtooth sequence $T[n]$; Illustration of MU deactivation/activation events. Time between subsequent spikes was shortened for illustration purposes; in reality, it comprises hundreds of time instants.

are usually not shorter than a certain duration called *refractory period*, further denoted as $t_{\text{R}}$, which is in the order of 30 ms [25], [26], [27]. Thus, a spike train can be represented as a $0-1$ sparse process $U_i[n]$ (see Figure 1), where $n \in \mathbb{Z}$ is a discrete time instant, $i$ stands for the MU index, and 1 corresponds to the $i$-th MU's spike at instant $n$.

Each MN's spike causes a short contraction of its muscle fibers. This is accompanied by a discharge wave propagating along the muscle fibers from the axon's connection point at the neuromuscular junction to the muscle tendons. This process induces an electric potential difference on a pair of electrodes placed in the vicinity of the muscle fiber. Together, fibers of a MU induce a waveform, approximately 2.5-10 ms long, called the motor unit action potential (MUAP) and denoted as $H_i$.

Contributions from multiple MUs, whose muscle fibers are in the vicinity of the electrode, sum up to generate the EMG signal. EMG, further denoted as $(Y[n])_{n\in\mathbb{Z}}$, can be represented as a convolution [28], [29]:

$$Y[n] = \sum_{i \in A[n]} (H_i * U_i)[n] + W[n] \tag{1}$$

where $A[n]$ is the set of indexes of active MUs at time $n$; $W[n]$ is a noise process representing all errors between the actual data and the model output.

$H_i[n]$ can be considered a finite impulse response with maximal length $\ell_{\text{IR}}$. Initially, we will consider it constant over time (its tracking algorithm will be presented in part III-G):

$$H_i[n] \equiv H_i^* \tag{2}$$

Due to the fact that the refractory period $t_{\text{R}}$ is longer than a MUAP, we suppose that there is no overlapping between $H_i$ occurrences from the same MU $i$.

The vector of MUs' indexes $A[n]$, as noted before, represents the set of MUs that are active at the time instant $n$. Its transition model is described in section II-B2. We also

introduce the vector $(T_i[n])_{i\in A[n]}$, related to $U_i[n]$, with the following formulation:

$$T_i[n] = \begin{cases} 0 & \text{if } U_i[n] = 1 \\ T_i[n-1]+1 & \text{if } U_i[n] = 0 \end{cases} \quad (3)$$

Thus, $(T_i[n])_{i\in A[n]}$ is a discrete sawtooth sequence that characterizes the time passed since the previous spike (see Figure 1).

We also introduce $\Theta_i[n]$, a vector containing the parameters of $i$-th MU's spike train statistics. In our approach, we use the discrete Weibull probability density function (PDF) to model the inter-spike intervals (ISI) distribution, which is described by a scale parameter and a shape parameter, denoted here as $t_i[n]$ and $\beta_i[n]$. Initially, $\Theta[n]$ is assumed to be constant (its tracking algorithm will be presented in part III-G).

$$\Theta_i[n] \equiv \Theta_i^* \quad (4)$$

### B. State vector and transition laws of HMM

The notation and the linear model of iEMG presented above permits to establish a hidden Markov model (HMM) with the following state vectors:

- $S[n] = (A[n], (T_i[n])_{i\in A[n]})$ the activation scenario,
- $H[n] = (H_i[n])_{i\in\Omega}$ the MUAP shapes,
- $\Theta[n] = (\Theta_i[n])_{i\in\Omega}$ the inter-spike law parameters.

where $\Omega$ denotes the set of all MUs, including active and inactive ones.

The transition laws for $H_i[n]$ and $\Theta_i[n]$ are derived from (2) and (4):

$$H_i[n+1] = H_i[n] \quad (5)$$
$$\Theta_i[n+1] = \Theta_i[n] \quad (6)$$

Although state vectors $H[n]$ and $\Theta[n]$ are considered stationary, practically it is never the case. An adaptation to steady changes of these parameters will be introduced later in this article (see III-G). Transition laws for $S[n] = (A[n], (T_i[n])_{i\in A[n]})$ are presented in the following two subsections, respectively for the two components $T_i[n]$ and $A[n]$.

*1) Renewal model for spike trains:* For each active MU $i$, inter-spike intervals $\Delta_i$ are supposed to be independent identically distributed random variables, with a parameterized probability mass function (PMF) $\mathsf{Pr}(\Delta_i = t \mid \Theta_i^*)$, for all natural numbers $t \geq 1$.

A probability law can also be represented by the reliability function $s$ or the hazard rate $r$ [30]:

$$s(t, \Theta_i^*) = \mathsf{Pr}(\Delta_i \geq t \mid \Theta_i^*) \quad (7)$$
$$r(t, \Theta_i^*) = \mathsf{Pr}(\Delta_i = t \mid \Delta_i \geq t, \Theta_i^*) \quad (8)$$

And it can be characterized by its mean value $m$:

$$m(\Theta_i^*) = \mathsf{E}(\Delta_i \mid \Theta_i^*)$$

where $\mathsf{E}(.)$ stands for the expectation.

As shown in [23], the process $(T_i[n])_{n\in\mathbb{Z}}$ is Markovian; its transition distribution is, for each $i \in A[n+1] \cap A[n]$:

$$T_i[n+1] = \begin{cases} 0 & \text{w.p. } r(T_i[n]+1, \Theta_i[n]) \\ T_i[n]+1 & \text{w.p. } 1 - r(T_i[n]+1, \Theta_i[n]) \end{cases} \quad (9)$$

The invariant distribution is:

$$\mathsf{Pr}(T_i[n] = t \mid \Theta_i[n]) = \frac{s(t+1, \Theta_i[n])}{m(\Theta_i[n])} \quad (10)$$

As in [23], a discrete Weibull distribution [31] for the interspike interval (with two parameters: $t_0$ a location one, and $\beta$ a concentration one) is chosen; for all $t > t_{\text{R}}$:

$$\mathsf{Pr}(\Delta_i = t \mid \Theta_i^* = (t_0, \beta)) = \exp\left[-\left(\frac{t-1-t_{\text{R}}}{t_0 - t_{\text{R}}}\right)^{\beta}\right] - \exp\left[-\left(\frac{t-t_{\text{R}}}{t_0 - t_{\text{R}}}\right)^{\beta}\right] \quad (11)$$

The hazard rate and the reliability function can be easily derived from (11). Also, a reasonable approximation of the mean ISI can be obtained [23].

*2) Recruitment model:* As it was mentioned above, the regulation of muscle contraction force is achieved by concurrent modulation of MN firing frequencies (rate coding) and recruitment. The recruitment mechanism is introduced into our model using the vector $A[n]$ containing the indexes of all MUs that are active at the time instant $n$. It has the following transition law:

$$A[n+1] = \begin{cases} A[n] \setminus i & \text{w.p. 1, if } T_i[n] = t_I \\ A[n] \cup i & \text{w.p. } \frac{\lambda}{\text{card}(\bar{A}[n])}, \text{ if i} \notin A[n] \end{cases} \quad (12)$$

where $\text{card}(A[n])$ denotes the number of active MUs indexes in $A[n]$.

In this way the $i$-th active MU is considered to be derecruited when the time passed since its previous spike $T_i[n]$ reaches a predefined limit $t_{\text{I}}$ (see Figure 1). A random inactive MU is considered recruited with predefined probability $\lambda$. Thus, $1-\lambda$ is the probability of not activating any MUs at time instant $n$. Newly recruited MUs are initialized with $T_i[n+1] = 0$.

### C. Observation model

The observation equation can be derived from (1):

$$Y[n] = \sum_{i\in\Omega} \varphi_i(S[n])\, H_i[n] + W[n] \quad (13)$$

where for all $s = (a, (t_j)_{j\in a})$, $\varphi_i(s)$ is a row vector of size $\ell_{\text{IR}}$ with all components equal to zero, except, if $i \in a$ and $t_i < \ell_{\text{IR}}$, the component in position $t_i + 1$ has value 1. The additive noise $(W[n])_{n\in\mathbb{Z}}$ is assumed zero-mean independent and identically distributed Gaussian process, with unknown variance $v$.

## III. Bayes filter

### A. Principle

The Bayes filter propagates the posterior probability law of the state sequence of an HMM along time. In the sequel, the exponent $^n$ means "from 1 to $n$" (e.g. $Y^n = [Y[1], Y[2], ..., Y[n]]$), and the exponent $^{|n}$ means "given the data $Y^n$". For a growing time index $n$, we have to compute:

- The posterior probability density function (PDF) of $\Theta[n]$ given $S^n, Y^n, H$. Obviously, given $S^n$, observation $Y^n$ and impulse response $H$ do not bring any information

about $\Theta[n]$. Furthermore, due to MUs independence, its PDF is the product of the PDF of $\Theta_i[n]$ given $S^n$.
In the approximate Bayes estimator that we will propose in the following, only the computation of the expected value of $\Theta_i$ given $S^n$ is needed. It will be approximated by using a recursive maximum likelihood estimation and noted $\hat{\theta}_{i,S^n}$ (see part III-B)

- The PDF of $H[n]$ given $S^n$ and $Y^n$. Thanks to the marginalization principle [32], this PDF is Gaussian and is computed using Kalman filter. The mean and the variance of this PDF will be denoted $\hat{H}^{|n}_{S^n}$ and $P_{S^n}$. Furthermore, the Kalman filter provides an observation prediction noted as $\hat{Y}^{|n-1}_{S^n}$, as well as its variance noted as $v_{S^n}$ (see part III-C).
- The PMF of $S^n$ given $Y^n$ (see part III-D). We should notice that it is impossible to process all possible values of $S^n$, since their number increases exponentially as the time index $n$ grows. The $n_{\text{path}}$ most probable paths are kept at every time index, where $n_{\text{path}}$ is chosen according to the available computation power.

### B. Estimation of the inter-spike law parameters

To estimate the inter-spike law parameters (parameters of the discrete Weibull distribution), a recursive maximum likelihood (RML) estimator is implemented. The likelihood is optimized iteratively by the quasi-Newton method.

For all $n \geq 1$, if $i \in A[n] \cap A[n-1]$, we define an active time index $\tau$:

$$\tau_{i,S^n} = \begin{cases} \tau_{i,S^{n-1}} + 1 & \text{if } i \in A[n] \\ \tau_{i,S^{n-1}} & \text{if } i \notin A[n] \end{cases} \tag{14}$$

Then, for the estimation of an $i$-th MU inter-spike law parameters vector $\theta$, we have:

$$\hat{\theta}_{i,S^n} = \hat{\theta}_{i,S^{n-1}} - \frac{1}{\tau_{i,S^n}}\ G^{-1}_{i,S^n}\ Q'_{i,S^n}(\hat{\theta}_{i,S^{n-1}}) \tag{15}$$

$$\begin{aligned} G_{i,S^n} =& \frac{1}{\tau_{i,S^n}}[Q'_{i,S^n}(\hat{\theta}_{i,S^{n-1}})][Q'_{i,S^n}(\hat{\theta}_{i,S^{n-1}})]^\top + \\ & (1 - \frac{1}{\tau_{i,S^n}})\ G_{i,S^{n-1}} \end{aligned} \tag{16}$$

Where $G_{i,S^n}$ is the approximate Hessian matrix of the maximum likelihood criterion $Q_{i,S^n}(\theta)$ at the current estimate, and $Q'_{i,S^n}(\theta)$ is its gradient with:

$$Q_{i,S^n}(\theta) = \begin{cases} -\ln(r(t_i[n]+1,\theta)) & \text{if } t_i[n+1] = 0 \\ -\ln(1-r(t_i[n]+1,\theta)) & \text{if } t_i[n+1] = t_i[n]+1 \end{cases}$$

If $i \notin A[n] \cap A[n-1]$, we assume:

$$\begin{cases} \hat{\theta}_{i,S^n} = \hat{\theta}_{i,S^{n-1}} \\ G_{i,S^n} = G_{i,S^{n-1}} \end{cases} \tag{17}$$

Expression (17) fits to the assumption that we have previously made about the stationarity of Weibull parameters (4).

The justification of the Weibull parameters estimation procedure is shown in the appendix A.

### C. Estimation of impulse responses

Given $S^n$, the Markov model for impulse responses reduces, for all $n \geq 1$:

$$\begin{cases} H[n+1] = H[n] \\ Y[n] = \sum_{i \in \Omega} \varphi_i(S[n])\ H_i[n] + W[n] \end{cases} \tag{18}$$

Where $W[n]$ assumed to be an independent and identically distributed Gaussian white noise with variance $v$. $H[1]$ and $H[n] \mid S^n, Y^n$ are Gaussian with means $\hat{H}^{|n}_{S^n}$ and covariance matrices $P_{S^n}$. $Y[n] \mid S^n, Y^{n-1}$ is Gaussian with mean $\hat{Y}^{|n-1}_{S^n}$ and variance $v_{S^n}$. These means and variances can be estimated recursively by Kalman filter. With the initial prior $\hat{H}^{|0}_{S^0}$ and $P_{S^0}$, we have, for all $n \geq 1$:

- Prediction of observation:

$$\begin{aligned} \hat{Y}^{|n-1}_{S^n} &= \psi(S[n])\ \hat{H}^{|n-1}_{S^{n-1}} \\ v_{S^n} &= \psi(S[n])\ P_{S^{n-1}}\ \psi(S[n])^\top + v \end{aligned} \tag{19}$$

- Estimation of state:

$$\begin{aligned} K_{S^n} &= P_{S^{n-1}}\ \psi(S[n])^\top\ v^{-1}_{S^n} \\ \hat{H}^{|n}_{S^n} &= \hat{H}^{|n-1}_{S^{n-1}} + K_{S^n}\ (Y[n] - \hat{Y}^{|n-1}_{S^n}) \\ P_{S^n} &= P_{S^{n-1}} - K_{S^n}\ v_{S^n}\ K^\top_{S^n} \end{aligned} \tag{20}$$

Where $K_{S^n}$ is the Kalman gain and $\psi(s) = [\varphi_1(s), ..., \varphi_{\text{card}(a[n])}(s)]$.

Moreover, the variance $v$ of noise is unknown. An heuristic approach is proposed to estimate it with the square of the residual $Y[n] - \psi(S[n])\hat{H}^{|n}_{S^n}$.

$$\hat{V}^{|n}_{S^n} = (1 - \frac{1}{n})\hat{V}^{|n-1}_{S^{n-1}} + \frac{1}{n}(Y[n] - \psi(S[n])\ \hat{H}^{|n}_{S^n})^2 \tag{21}$$

And the global estimation is:

$$\hat{V}^{|n} = \sum_{S^n}\ \hat{V}^{|n}_{S^n}\ \mathsf{Pr}^{|n}(S^n = s^n) \tag{22}$$

Where $\hat{V}^{|n}$ replaces $v$ in the formula (19).

### D. Posterior probability of scenario

The posterior probability recursion is derived by means of an update-prediction scheme. According to the Bayes rule, for all possible realizations $s^n$ of $S^n$, the update step is:

$$\mathsf{Pr}^{|n}(S^n = s^n) \propto \mathsf{Pr}^{|n-1}(S^n = s^n)\ g(Y[n] - \hat{Y}^{|n-1}_{s^n}, v_{s^n}) \tag{23}$$

Where $g(.\,, v)$ is the zero-mean and variance $v$ Gaussian PDF. The prediction step is:

$$\begin{aligned} &\mathsf{Pr}^{|n}(S^{n+1} = s^{n+1}) = \mathsf{Pr}^{|n}(S^n = s^n) \times \\ &\mathsf{Pr}(A[n+1] = a[n+1] \mid S[n] = s[n]) \times \\ &\prod_{i \in A[n+1]} \mathsf{Pr}(T_i[n+1] = t_i[n+1] \mid S^n = s^n) \end{aligned} \tag{24}$$

Where $\mathsf{Pr}(A[n+1] = a[n+1] \mid S[n])$ is the transition probability of the recruitment model. The elements $\mathsf{Pr}(T_i[n+1] = t_i[n+1] \mid S^n)$, for all $i \in A[n+1]$, are differently calculated:

If $i \in A[n+1] \cap A[n]$, meaning that the MU is already active, using the total probability formula and the Markov assumption, we have:

$$\begin{aligned}&\mathsf{Pr}(T_i[n+1] = t_i[n+1] \mid S^n)\\ &= \mathsf{E}(\mathsf{Pr}(T_i[n+1] = t_i[n+1] \mid \Theta_i[n], S^n) \mid S^n)\\ &= \mathsf{E}(\mathsf{Pr}(T_i[n+1] = t_i[n+1] \mid T_i[n], \Theta_i[n]) \mid S^n)\end{aligned} \tag{25}$$

With regard of the transition law of sawtooth sequence, we have:

$$\mathsf{Pr}(T_i[n+1] = t_i[n+1] \mid S^n) = \begin{cases}\mathsf{E}(r(T_i[n]+1, \Theta_i[n]) \mid S^n) & \text{if } t_i[n+1] = 0\\ 1 - \mathsf{E}(r(T_i[n]+1, \Theta_i[n]) \mid S^n) & \\ & \text{if } t_i[n+1] = T_i[n]+1\\ 0 & \text{otherwise}\end{cases} \tag{26}$$

We make a strong assumption that the expected hazard rate of the random parameter is the hazard rate of the expected parameter.

$$\mathsf{Pr}(T_i[n+1] = t_i[n+1] \mid S^n) \approx \begin{cases}r(T_i[n]+1, \mathsf{E}(\Theta_i[n+1] \mid S^n)) & \text{if } t_i[n+1] = 0\\ 1 - r(T_i[n]+1, \mathsf{E}(\Theta_i[n+1] \mid S^n)) & \\ & \text{if } t_i[n+1] = T_i[n]+1\\ 0 & \text{otherwise}\end{cases} \tag{27}$$

And the expected parameter is approximated by its RML estimate $\hat{\theta}_{i,S^n}$ provided in part III-B.

$$\mathsf{Pr}(T_i[n+1] = t_i[n+1] \mid S^n) \approx \begin{cases}r(T_i[n]+1, \hat{\theta}_{i,S^n}) & \text{if } t_i[n+1] = 0\\ 1 - r(T_i[n]+1, \hat{\theta}_{i,S^n}) & \text{if } t_i[n+1] = T_i[n]+1\\ 0 & \text{otherwise}\end{cases} \tag{28}$$

If $i \in A[n+1] \backslash A[n]$, meaning that the MU is activated at the time index $n+1$ with $T_i[n+1] = 0$ (as presented in the II-B2), the transition law $T_i[n+1] \mid \Theta_i$ is not influenced by the inter-spike distribution parameters due to the lack of the information about them. Thus, we set:

$$\mathsf{Pr}(T_i[n+1] = 0 \mid S^n) = 1 \tag{29}$$

### *E. Initialisation*

At the beginning of the decomposition, we assume that there is no active MUs. Therefore, the set of active MUs indexes $A[1]$ and the sawtooth sequence $T[1]$ are empty. Estimates of the impulse responses are manually or automatically extracted using other techniques, e.g. proposed in [15], [33], [34]. The algorithm is initialized with their rough versions $\hat{H}^{|0}_{S^1}$, here deteriorated by random shifts and additive noise to demonstrated the adaptability of the algorithm to variations in these estimates. Covariance matrices of impulse responses $P_{S^0}$ are initialized as diagonal with standard deviations set to 10 % of a corresponding value from $H_i$. An initial estimation of the noise variance $\hat{V}^{|0}_{s^0}$ is made using a signal extract containing no spikes. The initial ISI distribution law parameters of active MUs $\hat{\theta}_{i,S^0}$ are composed of $t_0$ (typically $3t_R \sim 4t_R$) and $\beta$ (typically $2 \sim 4$) according to our experience. Finally, $n_{\text{path}}$ initial $S^1$ are weighted with the same initial probability $\mathsf{Pr}^{|0}(S^1 = s^1)$.

### *F. Bayes estimator*

During the decomposition, at every time index the algorithm chooses $n_{\text{path}}$ most probable paths and discards the rest. The probabilities of the retained paths are used as weights to derive the Bayes state estimators, that is:

- A marginal maximum a posteriori (MAP) estimator for the sawtooth sequences and the set of active MUs. The most probable path provides the output spike trains:

$$\hat{S}^{n|n} = \arg\max_{s^n} \mathsf{Pr}^{|n}(S^n = s^n) \tag{30}$$

- The minimum mean square error estimator for the impulse responses and the interspike law parameters. Using the total expectation formula:

$$\begin{aligned}\hat{H}^{|n} =& \mathsf{E}^{|n}(H) = \mathsf{E}^{|n}(\mathsf{E}^{|n}(H \mid S^n))\\ =& \sum_{s^n} \underbrace{\mathsf{E}^{|n}(H \mid S^n = s^n)}_{\hat{H}^{|n}_{s^n}} \mathsf{Pr}^{|n}(S^n = s^n)\end{aligned} \tag{31}$$

$$\hat{\Theta}^{|n}_i = \sum_{s^n} \underbrace{\mathsf{E}^{|n}(\Theta_i \mid S^n = s^n)}_{\hat{\theta}_{i,s^n}} \mathsf{Pr}^{|n}(S^n = s^n) \tag{32}$$

### *G. Tracking*

The inter-spike laws parameters and the impulse responses are known to be time varying. To set the adaptivity of Bayes filter, we introduce the window length sequence $\ell[n]$ growing from 1 to the maximum window length $\ell_\infty$ with the recursion formula [35]:

$$\begin{cases}\ell[1] = 1\\ \ell[n+1] = (1 - \frac{1}{\ell_\infty})\ \ell[n] + 1\end{cases} \tag{33}$$

Where the maximum window length $\ell_\infty$ is related to the desired adaptivity. If $\ell_\infty = +\infty$, there is no tracking.

With the adaptivity coefficients, the formula of the estimated variance of noise (21) is rewritten as:

$$\hat{V}^{|n}_{S^n} = (1 - \frac{1}{\ell[n]})\hat{V}^{|n-1}_{S^{n-1}} + \frac{1}{\ell[n]}(Y[n] - \psi(S[n])\ \hat{H}^{|n}_{S^n})^2 \tag{34}$$

For the inter-spike law parameters estimation, considering the activation-inactivation of each MU, the window length sequence is slightly different:

$$\tau_{i,S^n} = \begin{cases}(1 - \frac{1}{\ell_\infty})\ \tau_{i,S^{n-1}} + 1 & \text{if } i \in A[n]\\ \tau_{i,S^{n-1}} & \text{if } i \notin A[n]\end{cases} \tag{35}$$

We replace the active index (14) by the adaptive formula (35).

Furthermore, as the operation shown in [36], to artificially increase the covariance matrix in the Kalman filter, the maximum window length is applied to the formula of estimation of state (20):

$$P_{S^n} = \frac{1}{1 - \frac{1}{\ell_\infty}}(P_{S^{n-1}} - K_{S^n}\ v_{S^n}\ K^\top_{S^n}) \tag{36}$$

### *H. Outline of the algorithm*

An outline of the proposed decomposition method is presented in Algorithm 1.

**Algorithm 1** Full estimation process

Initialize $\hat{H}^{|0}_{s^0}$, $P_{s^0}$, $\hat{V}^{|0}_{s^0}$, $\hat{\theta}_{i,s^0}$, $G_{i,s^0}$ and $s^1$
**for** all initial $s[1]$ **do**
  Initialize $\mathsf{Pr}^{|0}(S^1 = s^1)$
  Predict $\hat{Y}^{|0}_{s^1}$ and $v_{s^1}$ with (19)
**end for**
**for** all $n \geq 1$ **do**
  **new data** $Y[n]$
  **for** all $s^n$ **do**
    Compute the posterior $\mathsf{Pr}^{|n}(S^n = s^n)$ with (23)
  **end for**
  Select and keep the $n_{\text{path}}$ most probable paths
  **for** all $s^n$ **do**
    Update $\hat{H}^{|n}_{s^n}$ and $P_{s^n}$ with (20) (corrected by (36))
    Update $\hat{V}^{|n}_{s^n}$ with (34)
  **end for**
  **for** all $s^n$ **do**
    **if** source $i \notin a[n] \cap a[n-1]$ **then**
      Update $\hat{\theta}_{i,s^n}$ and $G_{i,s^n}$ with (17)
    **else**
      Update $\hat{\theta}_{i,s^n}$ and $G_{i,s^n}$ with (15) and (16)
    **end if**
  **end for**
  Compute $\hat{H}^{|n}$, $\hat{\Theta}^{|n}_i$ and $\hat{V}^{|n}$ with (31), (32), and (22)
  **for** all $s^n$ **do**
    **if** $t_i[n] = t_I$ **then**
      Drop $t_i[n]$ from $t[n]$ and update $a[n+1]$
    **else**
      Draw $\alpha$ from a uniform distribution $[0, 1]$
      **if** $\alpha < \lambda$ **then**
        Activate a random source from $\bar{a}[n]$
        Initialize its value in $t[n]$ and update $a[n+1]$
      **end if**
    **end if**
    Compute $\mathsf{Pr}(A[n+1] = a[n+1] \mid S[n] = s[n])$
  **end for**
  **for** all kept $(t^n, a^{n+1})$ **do**
    **for** all possible forks $t^{n+1}$ from $t^n$ **do**
      Compute $\mathsf{Pr}^{|n}(S^{n+1} = s^{n+1})$ with (24) and (27)
    **end for**
    Predict $\hat{Y}^{|n}_{s^{n+1}}$ and $v_{s^{n+1}}$ with (19)
  **end for**
**end for**

## IV. Experimental and simulation protocols

### A. Signals

The algorithm was evaluated using simulated and experimental iEMG signals. Simulated signals were generated by the described Markov model with sampling frequency of 5 kHz and duration 20 s. MUAP shapes for the simulations were obtained from experimental iEMG signals that were manually decomposed. The value of the refractory period was chosen to be 30 ms. For the Weibull distribution, the location parameter $t_0$ ranged from 60 ms to 90 ms and the concentration parameter $\beta$ ranged from 2 to 6. The SNR (Signal to Noise Ratio) was set to 10 dB. Three groups of signals were simulated with respectively 6, 8 and 10 MUs. In each group, there were 10 signals.

Experimental signals were acquired from two muscles. A set of fine-wire experimental iEMG was acquired from the tibialis anterior (TA) muscle of a 26 years-old healthy man. The subject was asked to perform three trials of an isometric force tracking task of 24 s duration. The force profile was trapezoidal with target force set to 20% of the maximal voluntary contraction (MVC). The wire electrodes used for these recordings were made of Teflon coated stainless steel (50 um diameter; A-M Systems, Carlsborg, WA, USA) and inserted into the muscle with 25G needles.

A second set of experimental signals was acquired from the abductor digiti minimi (ADM) muscle of a healthy 28 years-old man with a needle electrode (30G Myoline disposable concentric needle) inserted in the muscle belly at a depth of 4-6 mm. The full abduction range of the little finger (45 degrees) was divided into five equiangular positions (including the maximal abduction and excluding full adduction). The subject was asked to perform a muscle contraction at low muscle activation level (subjective) in each position while being given a visual feedback on the recorded signal.

Since the algorithm initialized all MUs as inactive, the onset of the experimental signal was associated to a recruitment of all MUs at once, which does not prevent the algorithm from converging to the correct state, as will be shown later.

The signals from TA and ADM were amplified, band-pass filtered between 100 Hz and 4.4 kHz and sampled at a frequency of 10kHz using "MEBA" EMG amplifier (OT Bioelettronica, Torino, Italy). The signals from TA were subsequently down-sampled to 5 kHz.

Algorithm 1 was applied to decode the simulated and the experimental signals. The activation probability $\lambda$ and the maximum time $t_I$ were respectively set to 0.03 and $7t_R$; The window length corresponding to the adaptivity was 1.4 s. The number of selected paths was set to 128, 256 and 384 for the simulated signal and 512 for the experimental signal.

### B. Indexes of performance and complexity

Automatic decomposition results were evaluated in terms of spike train similarity relatively to the reference decomposition. In the case of experimental signals, the reference was an expert-provided manual decomposition using EMGLAB [37]. In case of simulated signals, the exact spike trains used in the simulation were known.

First, to characterize the decomposition problem complexity, we introduce a superposition percentage Sup:

$$\text{Sup} = \frac{Nb_{sup}}{Nb_{spikes}} \tag{37}$$

where $Nb_{spikes}$ is the overall number of spikes in the reference train; $Nb_{sup}$ is the number of spikes that are involved in superpositions. We considered a MUAP superimposed with others if there was at least one other MUAP closer than 3 ms to it. This value was chosen as half of the average MUAP duration that we usually observed in experimental signals.

TABLE II: Decomposition performance for simulated signals: 'Nb MUs' is the maximal number of MUs concurrently active in the signal; 'Nb sup-spikes' represents the number of spikes involved in superpositions; 'Nb spikes' denotes the overall number of spikes in the signal; 'Sup.' is the percentage of superposition; 'Nb paths' is the number of paths used in the algorithm; 'Sens.' denotes the global sensitivity; 'Pred.' is the global predictivity.

| Nb MUs | Nb sup-spikes | Nb spikes | Sup.(%) | Nb paths | Sens. (%) | Pred. (%) |
|---|---|---|---|---|---|---|
| 10 | 661±66.59 | 2159.20±120.07 | 30.61±3.08 | 384 | 95.05±2.39 | 91.95±3.13 |
| | | | | 256 | 91.78±4.54 | 88.30±5.15 |
| | | | | 128 | 82.94±7.14 | 77.59±7.20 |
| 8 | 452.40±33.65 | 1810.40±44.09 | 24.99±1.86 | 384 | 96.86±1.63 | 94.46±2.76 |
| 6 | 275.60±16.06 | 1445.40±48.87 | 19.07±1.11 | 384 | 99.11±0.83 | 98.65±1.35 |

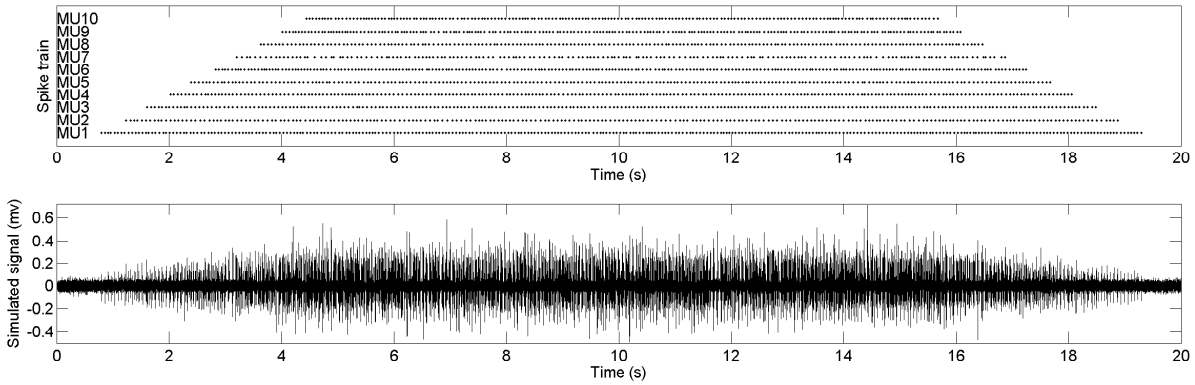


Fig. 2: Example of a simulated signal with 10 MUs: The recruitment profile is shown in the upper panel. Corresponding simulated signal with 10 dB SNR is depicted in the lower panel.

TABLE III: Decomposition performance for experimental signals: 'TA' and 'ADM' respectively represent signals from the tibialis anterior and abductor digiti minimi; 'Position' represents the level of abduction scaled equiangularly from the full adduction (0, not included) to the full abduction (5); 'Nb MUs' is the maximal number of MUs concurrently active in the signal; 'Sens.' and 'Pred.' represent respectively the global sensitivity and predictivity as estimated by comparison with the manual expert decomposition; 'NB spikes' represents the overall number of spikes in the signal; and 'Sup.' is the percentage of superposition.

| Index | Muscle | Duration (s) | Force (MVC%) | Position | Nb MUs | Nb spikes | Sup.(%) | Sens. (%) | Pred.(%) |
|---|---|---|---|---|---|---|---|---|---|
| 1 | TA | 24 | 20 | - | 5 | 873 | 18.79 | 91.75 | 90.61 |
| 2 | TA | 24 | 20 | - | 5 | 936 | 17.52 | 95.83 | 94.72 |
| 3 | TA | 24 | 20 | - | 6 | 933 | 17.15 | 94.53 | 93.43 |
| 4 | ADM | 5 | - | 1 | 2 | 61 | 6.56 | 100 | 100 |
| 5 | ADM | 5 | - | 2 | 5 | 153 | 15.03 | 96.73 | 92.50 |
| 6 | ADM | 5 | - | 3 | 6 | 192 | 21.35 | 96.88 | 92.54 |
| 7 | ADM | 5 | - | 4 | 6 | 281 | 23.13 | 90.10 | 90.14 |
| 8 | ADM | 5 | - | 5 | 7 | 371 | 28.84 | 92.99 | 92.74 |

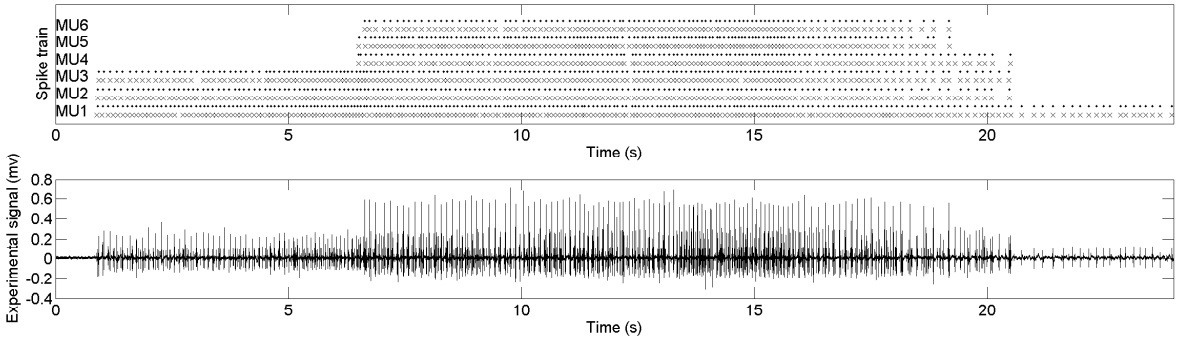


Fig. 3: Comparison of automatic (crosses, 'x') and reference (points, '.') decompositions (upper panel) and the experimental signal from TA, 20% MVC (lower panel).

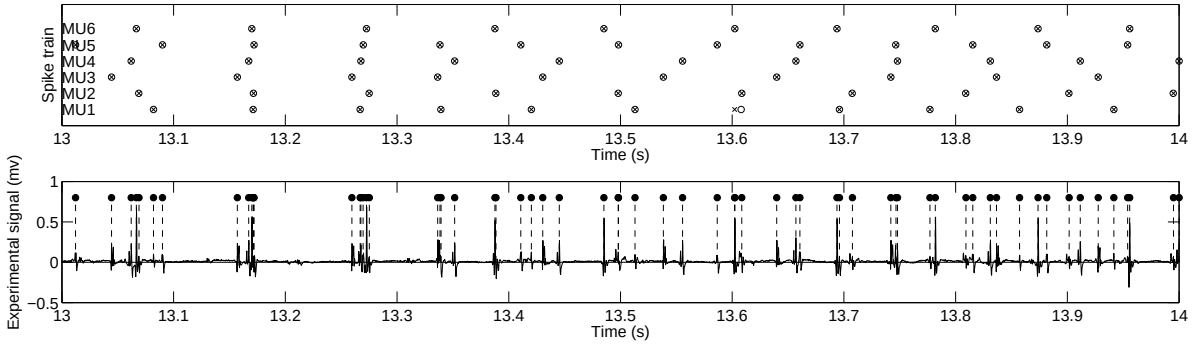


Fig. 4: An extract of the experimental signal decomposition shown in figure 3; circles 'o' and crosses 'x' represent respectively the spikes from the reference and automatic decompositions.

In order to quantitatively evaluate the decomposition results, we used global sensitivity and global positive predictivity values, defined as following. A MUAP was considered correctly identified (true positive) if the reference train contained a spike from the same MU within a margin of 1 ms around it. Thus, global sensitivity was defined as the overall number of correctly identified MUAPs from all MUs, divided by the overall number of spikes in the reference decomposition. Global positive predictivity was the number of correctly identified spikes divided by the overall number of spikes in the decomposition under evaluation.

We also performed an individual analysis of each MUAP train, using "classification phase" indexes proposed in [38]. These indexes included sensitivity, specificity and accuracy, as they are defined in [38].

## V. Results

### A. Simulated signals

As shown in Table II, three groups of simulated signals with 6, 8 and 10 MUs were decomposed. Their recruitment profile is shown in the upper panel of Figure 2, while an example of a signal with 10 MUs is provided in the lower panel.

We note that the mean values of global sensitivity and predictivity (Table II) decrease for signals with larger number of active MUs. This is due to the fact that the decomposition task becomes more complex in terms of overall number of spikes and of the superposition percentage. We also note the increase in standard deviations of the performance indexes, demonstrating the proportionality between task complexity and decrease in performance of the algorithm.

Signals containing 10 MUs were also decomposed using three different numbers of paths ($n_{path}$ in previous sections): 128, 256 and 384. Results in Table II show that the performance of the algorithm improved with the amount of used computational resources both in terms of accuracy and stability. The choice of maximal number of paths (384) was dictated by our current available computational resources.

### B. Experimental signals

Eight experimental signals (three recorded from the TA at 20% MVC and five detected from the ADM muscle in the five different abduction positions) were automatically decomposed. As shown in Table III, for these signals, the number of MU ranged from two to seven and the percentage of superposition ranged from 6% to 28%. For all these experimental signals, both the global sensitivity and predictivity were above 90%.

Detailed results of the decomposition are illustrated and analyzed in the following section for two representative signals: a fine-wire signal from the TA with 6 MUs and a needle signal from the ADM muscle with 7 MUs.

*1) Experimental signal with 6 MUs from the TA:* Figure 3 provides a global view of the decomposition results. In the upper panel, the activation zone of each MU in the decomposition algorithm is correlated with the manual reference, which proves that the recruitment model presented in part II is accurate.

To provide a detailed view of the decomposition results, we have chosen a one second extract of the signal, containing the most challenging superposition cases (see Figure 4). The algorithm performed generally well, successfully processing the complex superpositions of 5 MUs at a time (see signal between 13.1 and 13.3 seconds). It is also worth noting that a spike detection with limited precision, which occurred at 13.6 s, was recovered in the following firings of that MU.

The individual (per MU) performance indexes are shown in Table IV. The reason for the lower sensitivity in case of the first MU is the small amplitude of its MUAP, compared to the other ones. Generally, this can lead to its complete masking in the superpositions. However, the algorithm succeeded in tracking and decomposing this MU.

TABLE IV: Decomposition performance for an experimental signal detected from the TA with 6 MUs.

| MU | Sens. | Spec. | Acc. |
|---|---|---|---|
| MU1 | 89.66 | 96.56 | 94.84 |
| MU2 | 94.15 | 98.23 | 97.46 |
| MU3 | 97.67 | 99.72 | 99.32 |
| MU4 | 95.97 | 99.09 | 98.66 |
| MU5 | 94.74 | 98.05 | 97.57 |
| MU6 | 99.01 | 99.87 | 99.77 |

As shown in Section III-B, the algorithm recursively estimates the parameters of the discrete Weibull ISI distribution. Figure 5 shows the corresponding results for each MU in the

signal shown in Figure 3. Empirical firing rates were estimated as the inverse of the moving average of subsequent ISIs in the reference decomposition. The estimated firing rates were calculated via parameters $t_0$ and $\beta$ using the approximation proposed in [23]. The algorithm successfully tracked the changes in firing rates, including abrupt ones resulting from MU activation.

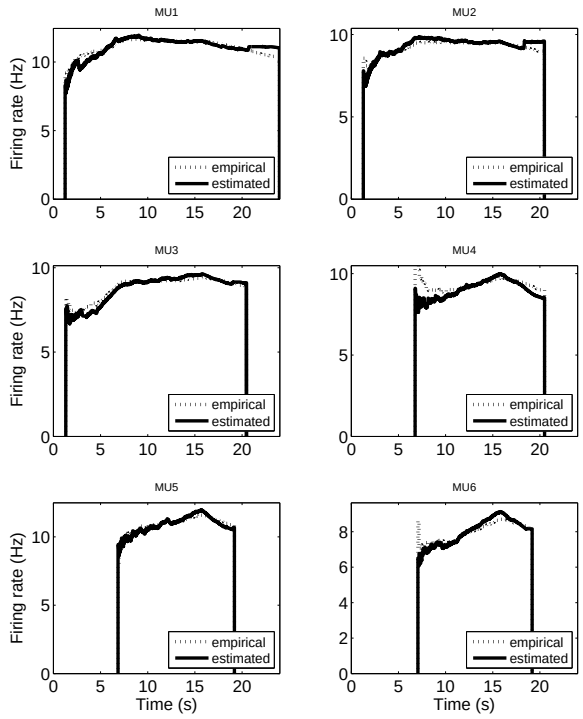


Fig. 5: Firing rates for the iEMG from TA set (see Figure 3): the dash line (empirical) represents the firing rates estimated using reference decomposition; continuous line (estimated) represents the firing rates calculated via parameters of discrete Weibull distribution estimated as described in Section (III-B).

TABLE V: Decomposition performance for an experimental signal (see Figure 6) from ADM set.

| MU | Sens. | Spec. | Acc. |
|---|---|---|---|
| MU1 | 81.69 | 97.29 | 94.26 |
| MU2 | 90.48 | 97.63 | 96.37 |
| MU3 | 98.33 | 99.31 | 99.14 |
| MU4 | 91.53 | 97.98 | 96.91 |
| MU5 | 100 | 100 | 100 |
| MU6 | 97.56 | 99.35 | 99.14 |
| MU7 | 100 | 99.37 | 97.42 |

*2) Experimental signal with 7 MUs from the ADM muscle:* Figure 6 shows an example of a 5 s signal recorded during maximal abduction of the little finger (approximately 45 degrees) and its decomposition results. Since the algorithm initializes all the MUs as inactive, the beginning of the signal is associated to the simultaneous activation of all MUs. We note that the algorithm successfully handled this condition, as well as sporadic activation of the 7th MU.

One second extracted from this signal is presented in Figure 7. All superposition cases, including complex ones (see signal at 3.1 s and at 3.85 s), were successfully decomposed.

The quantitative evaluation is provided in Table V. Compared to other MUs, the first is decomposed with relatively low specificity. Similarly to the previous case, this was due to the small size of its MUAP and its similarity to that of the second MU. This is illustrated in Figure 8 which provides the final estimates of the MUAP shapes and their initial values. It can be noted that the decomposition errors for the first MU mostly occur in the first half of the signal (Figure 6), while the remaining part of the signal is decomposed correctly. This case demonstrates the ability of the algorithm to converge to the correct solution over time due to the recursive upgrades of the ISI statistics and the impulse responses.

In order to illustrate the importance of the adaptation of the MUAP shapes, we have decomposed the same experimental signal with the Kalman filtering "switched off". In this case, the algorithm could not refine the initial rough estimates of the MUAPs and provided much lower sensitivity and predictivity values: 73.85% and 75.90% respectively. This result shows that the adaptation introduced by the Kalman filter is an important characteristic of the proposed algorithm.

Figure 9 shows the firing rates estimated from the reference decomposition ('empirical') and recursively by the algorithm ('estimated'). In this example, at first the firing rate of the 1st MU is underestimated due to several false negatives. However, the estimates recover later, establishing a correct tracking, in consistence with the results presented in Figure 6.

Finally, we have decomposed the same signal while fixing the number of active motor neurons, in order to replicate our previous approach for comparison [23]. With the previous approach, in these conditions, we have observed a divergence of the ISI distribution parameters of the MNs during the periods of their inactivity. This caused several false negatives at the very beginning of their activation, with subsequent slow convergence to a correct estimate of the state. Such errors are crucial when the onset of the contraction is of interest and can lead to an unrecoverable divergence in complex signals. This suggests that the introduction of the recruitment model critically improves the robustness of the algorithm.

## VI. Discussion and conclusion

An approximate Bayes filter was proposed, which permits to recursively decompose an iEMG signal, i.e estimate MUAP shapes, additive noise variance, ISI distribution parameters and track the activity of MNs. Simulated and experimental signal decompositions demonstrated the successful performance of the algorithm.

One of the limitations of the proposed approach is its dependence on manually-extracted MUAP dictionary. However, this task may be as well accomplished automatically using existing MUAPs clustering techniques. The algorithm is capable of correcting possible errors in initial MUAP estimates, as well as of tracking the subsequent gradual changes of MUAPs waveforms.

Another limitation of our approach is its computational complexity, which is $O(n_{\text{path}}(\text{card}(A[n+1])\ \ell_{\text{IR}})^2)$, leading to

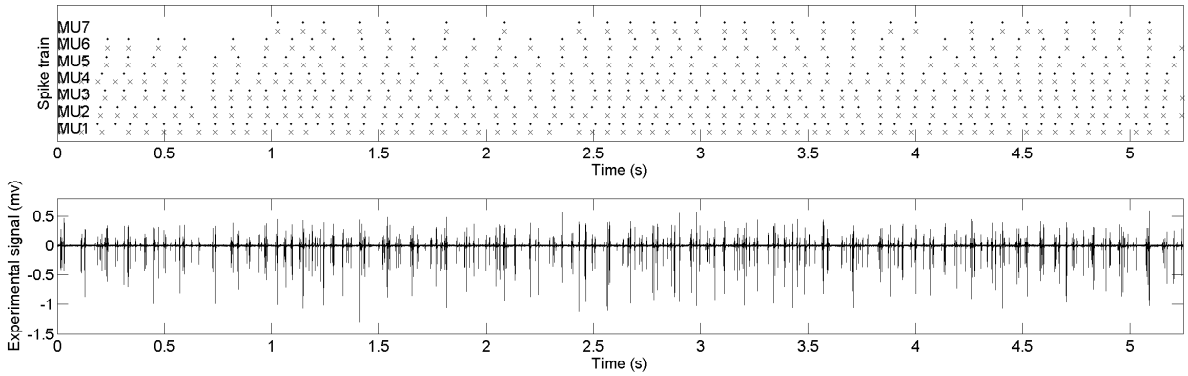


Fig. 6: Comparison of automatic (crosses, 'x') and reference (points, '.') decompositions (upper panel) and corresponding experimental signal from ADM, in position 5, corresponding to approximately 45 degrees of abduction (lower panel).

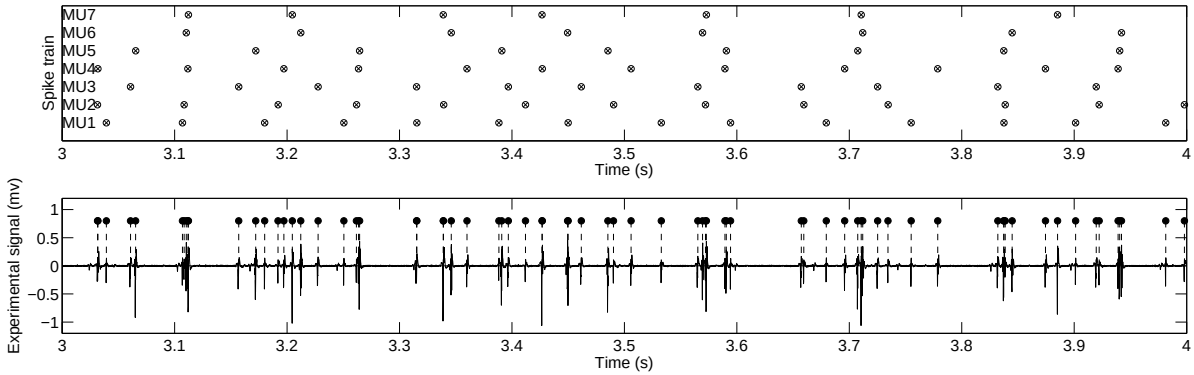


Fig. 7: An extract of the experimental signal decomposition shown in figure 6; circles '$\circ$' and crosses 'x' represent respectively the spikes from the reference and automatic decompositions.

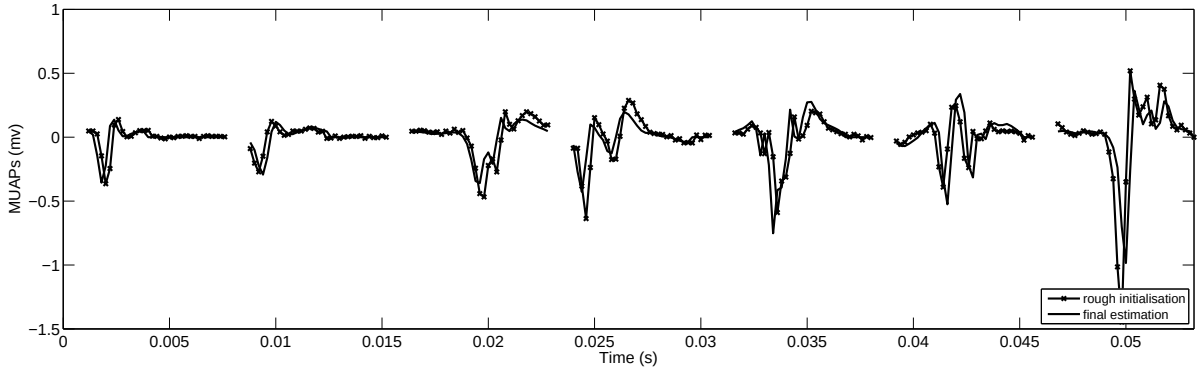


Fig. 8: Rough initial waveforms and final estimates of the MUAP waveforms, for the signal shown in Figure 7. For illustration purposes, the true waveforms are not shown, since they are not distinguishable from their final estimates, which indicates the effectiveness of the algorithm. The initial MUAP waveforms were manually extracted from the signal and then artificially deteriorated by adding noise and random temporal shifts.

high computation times in cases when $n_{path}$ should be large, i.e. when the number of active MUs is high. However, the algorithm can be efficiently parallelized due to the independence of the paths, which allows us to consider its parallel implementation for the future real-time application in human-machine interfaces.

Finally, the proposed algorithm allows the decomposition of signals with varying number of active motor units, which substantially broadens the domains of applicabitility of the

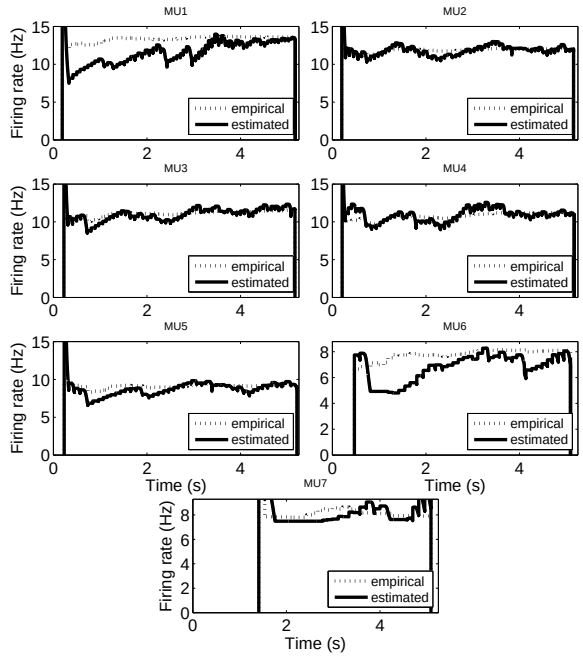


Fig. 9: Firing rates of the experimental signal with 7 MUs detected from ADM in the abduction position '5'

algorithm. We have shown that it successfully decomposes experimental signals acquired both with needle and fine-wire electrodes, during gradual and abrupt recruitments.

## APPENDIX A
## PROOF OF THE INTER-SPIKE LAW PARAMETERS ESTIMATION

To estimate the discrete Weibull distribution parameters, a maximum likelihood (ML) estimator is proposed in [39]. In [23], an online ML estimator is implemented. The likelihood is optimized iteratively by the quasi-Newton method. The ML of $\hat{\theta}_{i,S^n}$ is:

$$\hat{\theta}_{i,S^n} = \arg\min_{\theta} \underbrace{-\frac{1}{n} \ln \mathsf{Pr}(S^n = s^n \mid \Theta_i = \theta_i)}_{J_{i,S^n}(\theta)} \tag{38}$$

$J_{i,S^n}(\theta)$ is the objective function to minimize that is the great difference of this discrete Weibull distribution on-line ML estimator with others. In the classic discrete Weibull distribution ML estimators, $-\frac{1}{n} \ln \mathsf{Pr}(\triangle^n = l^n \mid \Theta_i = \theta_i)$ is usually interpreted as the objective function where $\triangle^n$ denotes the inter-spikes. The change of objective function leads to a practical on-line implementation.

Considering the Markov chain property of sawtooth sequences, the objective function $J_{i,S^n}(\theta)$ can be written for all $n \geq 1$:

$$\begin{aligned} J_{i,S^n}(\theta) =& \frac{1}{n} J_{i,S^1}(\theta) + \frac{1}{n} \sum_{k=2}^{n} Q_{i,S^n}(\theta) \\ J_{i,S^1}(\theta) =& -\ln \mathsf{Pr}(S[1] = s[1] \mid \Theta_i = \theta_i) \\ Q_{i,S^n}(\theta) =& -\ln \mathsf{Pr}(S[k] = s[k] \mid \Theta_i = \theta_i, S[k-1] = s[k-1]) \end{aligned} \tag{39}$$

where $J_{i,S^1}(\theta)$ and $Q_{S^n}(\theta)$ are computed by the formulas (9) and (10). The gradients of the two members of objective function are directly computed with the transition probability of the discrete Weibull law. The objective function is recursively minimized by a stochastic gradient update:

$$\hat{\theta}_{i,S^n} = \hat{\theta}_{i,S^{n-1}} - \frac{1}{n} G^{-1}_{i,S^n} Q'_{i,S^n}(\hat{\theta}_{i,S^{n-1}}) \tag{40}$$

Where $G_{i,S^n}$ is is an approximation of Hessian matrix obtained through the Fisher information matrix of the transition probability law [40], $Q'_{i,S^n}(\hat{\theta}_{i,S^{n-1}})$ is the partial derivative $Q_{i,S^n}$ with respect to the components of $\hat{\theta}_{i,S^{n-1}}$. For all $n \geq 2$, we have:

$$\begin{aligned} G_{i,S^n} =& \frac{1}{n}[Q'_{i,S^n}(\hat{\theta}_{i,S^{n-1}})][Q'_{i,S^n}(\hat{\theta}_{i,S^{n-1}})]^\top + \\ & (1 - \frac{1}{n}) G_{i,S^{n-1}} \end{aligned} \tag{41}$$

We notice that the approximation of Hessian matrix $G_{i,S^n}$ should be invertible in (40). If the matrix $G_{i,S^n}$ is not invertible, we update the inter-spike law parameters $\hat{\theta}_{i,S^n} = [\hat{t}_{0,i,S^n}; \hat{\beta}_{i,S^n}]$ using following formula:

$$\begin{aligned} \hat{t}_{0,i,S^n} =& \hat{t}_{0,i,S^{n-1}} - \frac{1}{n} \frac{Q'_{i,S^n}(\hat{t}_{0,i,S^{n-1}})}{G_{i,S^n}(1,1)} \\ \hat{\beta}_{i,S^n} =& \hat{\beta}_{i,S^{n-1}} \end{aligned} \tag{42}$$

Where $Q'_{i,S^n}(\hat{t}_{0,i,S^{n-1}})$ is the partial derivative $Q_{i,S^n}$ with respect to the components of $\hat{t}_{0,i,S^{n-1}}$, and $G_{i,S^n}(1,1)$ is the first element of the approximation of Hessian matrix $G_{i,S^n}$.

The estimation procedure should take into consideration the activation and deactivation of the source. In order to do that, we replace index $n$ by an active time index $\tau$ with following definition:

$$\tau_{i,S^n} = \begin{cases} \tau_{i,S^{n-1}} + 1 & \text{if } i \in A[n] \\ \tau_{i,S^{n-1}} & \text{if } i \notin A[n] \end{cases} \tag{43}$$

Moreover, we define that the estimated inter-spike law parameters and the approximation of Hessian matrix keep the same value as in previous time instant if the source is not active.

In conclusion, for all $n \geq 1$, we have:

- if $i \notin A[n] \cap A[n-1]$,

$$\begin{cases} \hat{\theta}_{i,S^n} = \hat{\theta}_{i,S^{n-1}} \\ G_{i,S^n} = G_{i,S^{n-1}} \end{cases} \tag{44}$$

- if $i \in A[n] \cap A[n-1]$ and $G_{i,S^n}$ is invertible,

$$\begin{aligned} \hat{\theta}_{i,S^n} =& \hat{\theta}_{i,S^{n-1}} - \frac{1}{\tau_{i,S^n}} G^{-1}_{i,S^n} Q'_{i,S^n}(\hat{\theta}_{i,S^{n-1}}) \\ G_{i,S^n} =& \frac{1}{\tau_{i,S^n}}[Q'_{i,S^n}(\hat{\theta}_{i,S^{n-1}})][Q'_{i,S^n}(\hat{\theta}_{i,S^{n-1}})]^\top + \\ & (1 - \frac{1}{\tau_{i,S^n}}) G_{i,S^{n-1}} \end{aligned} \tag{45}$$

- if $i \in A[n] \cap A[n-1]$ and $G_{i,S^n}$ is not invertible,

$$\begin{aligned}\hat{t}_{0,i,S^n} =& \hat{t}_{0,i,S^{n-1}} - \frac{1}{\tau_{i,S^n}} \frac{Q'_{i,S^n}(\hat{t}_{0,i,S^{n-1}})}{G_{i,S^n}(1,1)} \\ \hat{\beta}_{i,S^n} =& \hat{\beta}_{i,S^{n-1}} \\ G_{i,S^n} =& \frac{1}{\tau_{i,S^n}} [Q'_{i,S^n}(\hat{\theta}_{i,S^{n-1}})][Q'_{i,S^n}(\hat{\theta}_{i,S^{n-1}})]^\top + \\ & (1 - \frac{1}{\tau_{i,S^n}})\ G_{i,S^{n-1}}\end{aligned} \tag{46}$$

## ACKNOWLEDGMENT

This work was supported by the China Scholarship Council [grant number 201404490033] and by the University of Nantes as a part of project "Moderato".

## REFERENCES

[1] B. Mambrito and C. D. Luca, "A Technique for the Detection, Decomposition and Analysis of the EMG Signal," *Electroencephalography and Clinical Neurophysiology*, vol. 58, pp. 175–188, 1984.

[2] N. Miki, "Detailed analysis of clinical electromyography signals: EMG decomposition, findings and firing pattern analysis in controls and patients with myopathy and amytrophic lateral sclerosis," Ph.D. dissertation, University of Copenhagen, 2001.

[3] T. J. Doherty and D. W. Stashuk, "Decomposition-based quantitative electromyography: methods and initial normative data in five muscles," *Muscle Nerve*, vol. 28, pp. 204–211, 2003.

[4] T. Kamali, R. Boostani, and H. Parsaei, "A multiclassifier approach to MUAP classification for diagnosis of neuromuscular disorders," *IEEE Trans. on Neural Systems and Rehabilitation Engineering*, vol. 22, pp. 191–200, 2014.

[5] Z. C. Lateva, K. C. McGill, and M. E. Johanson, "The innervation and organization of motor units in a series-fibered human muscle: the brachioradialis," *European J. of Applied Physiology*, vol. 108, pp. 1530–1541, 2010.

[6] C. J. D. Luca and Z. Erim, "Common drive of motor units in regulation of muscle force," *Trends in Neurosciences*, vol. 17, pp. 299–305, 1994.

[7] A. Adam and C. J. D. Luca, "Recruitment order of motor units in human vastus lateralis muscle is maintained during fatiguing contractions," *Trends in Neurosciences*, vol. 90, pp. 2919–2927, 2003.

[8] D. Farina and A. Holobar, "Human machine interfacing by decoding the surface electromyogram," *IEEE Signal Processing Magazine*, vol. 32, pp. 115–120, 2015.

[9] F. Negro, S. Muceli, M. Castronovo, and D. Farina, "Multi-channel intramuscular and surface EMG decomposition by convolutive blind source separation," *J. of Neural Engineering*, vol. 13, no. 2, 2016.

[10] D. Farina, I. Vujaklija, and M. Sartori, "Man/machine interface based on the discharge timings of spinal motor neurons after targeted muscle reinnervation," *Nature biomedical engineering*, vol. 1, 2017.

[11] R. Merletti and D. Farina, "Analysis of intramuscular electromyogram signals," *Philosophical Trans. - Royal Society. Biological sciences*, vol. 367, pp. 357–368, 2009.

[12] V. J. Prochazka, B. Conrad, and F. Sindermann, "A neuroelectric signal recognition system," *Electroencephalography and Clinical Neurophysiology*, vol. 32, no. 1, pp. 95–97, 1972.

[13] V. J. Prochazka and H. H. Kornhuber, "On-line multi-unit sorting with resolution of superposition potentials," *Electroencephalography and Clinical Neurophysiology*, vol. 34, no. 1, pp. 91–93, 1973.

[14] J. F. Vibert and J. Costa, "Spike separation in multiunit records: A multivariate analysis of spike descriptive parameters," *Electroencephalography and Clinical Neurophysiology*, vol. 47, no. 2, pp. 172–182, 1979.

[15] J. Florestal, P. A. Mathieu, and A. Malanda, "Automated Decomposition of Intramuscular Electromyographic Signals," *IEEE Trans. on Biomedical Engineering*, vol. 53, no. 5, pp. 832–839, 2006.

[16] J. Florestal, P. Mathieu, and K. McGill, "Automatic decomposition of multichannel intramuscular EMG signals," *J. of Electromyography and Kinesiology*, vol. 19, pp. 1–9, 2009.

[17] H. R. Marateb, K. C. McGill, and A. Holobar, "Robust decomposition of single-channel intramuscular EMG signals at low force levels," *J. of Neural Engineering*, vol. 8, no. 6, p. 066015, 2011.

[18] D. Stashuk and H. DeBruin, "Automatic decomposition of selective needle-detected myoelectric signals," *IEEE Trans. on Biomedical Engineering*, vol. 35, pp. 1–10, 1988.

[19] S. Karimimehr, H. R. Marateb, S. Muceli, M. Mansourian, M. A. Mananas, and D. Farina, "A Real-Time Method for Decoding the Neural Drive to Muscles Using Single-Channel Intra-Muscular EMG Recordings," *Int. J. of Neural Systems*, vol. 27, no. 6, p. 1750025, 2017.

[20] A. Holobar and D. Zazula, "Multichannel blind source separation using convolution kernel compensation," *IEEE Trans. Signal Process*, pp. 55:4487–96, 2007.

[21] V. Glaser, A. Holobar, and D. Zazula, "Real-Time Motor Unit Identification From High-Density Surface EMG," *IEEE Trans. on Neural Systems and Rehabilitation Engineering*, vol. 21, no. 6, pp. 949–958, 2013.

[22] J. Roussel, P. Ravier, and M. Haritopoulos, "Decomposition of Multi-Channel Intramuscular EMG Signals by Cyclostationary-Based Blind Source Separation," *IEEE Trans. on Neural Systems and Rehabilitation Engineering*, vol. 25, no. 11, pp. 2035–2045, 2017.

[23] J. Monsifrot, E. Le Carpentier, Y. Aoustin, and D. Farina, "Sequential Decoding of Intramuscular EMG Signals via Estimation of a Markov Model," *IEEE Trans. on Neural Systems and Rehabilitation Engineering*, vol. 22, no. 5, pp. 1030–40, 2014.

[24] C. C.J. Heckman and R. Enoka, "Motor unit," *Compr Physiol*, vol. 2, no. 4, pp. 2629–2682, 2012.

[25] R. Betts, D. Johnston, and B. Brown, "Nerve fibre velocity and refractory period distributions in nerve trunks." *J. of Neurology, Neurosurgery & Psychiatry*, vol. 39, no. 7, pp. 694–700, 1976.

[26] J. Kimura, T. Yamada, and R. Rodnitzky, "Refractory period of human motor nerve fibres." *J. of Neurology, Neurosurgery & Psychiatry*, vol. 41, no. 9, pp. 784–790, 1978.

[27] D. Hampel and P. Lansky, "On the estimation of refractory period," *J. of Neuroscience Methods*, vol. 171, no. 2, pp. 288 – 295, 2008.

[28] D. Stashuk, "EMG signal decomposition: how can it be accomplished and used?" *J. of Electromyography and Kinesiology*, vol. 11, no. 3, pp. 151–173, 2001.

[29] D. Farina, A. Crosetti, and R. Merletti, "A model for the generation of synthetic intramuscular EMG signals to test decomposition algorithms," *IEEE Trans. on Biomedical Engineering*, vol. 48, no. 1, pp. 66–77, Jan. 2001.

[30] V. Barbu and N. Limnios, "Reliability theory for discrete-time semi-Markov systems," in *Semi-Markov Chains and Hidden Semi-Markov Models toward Applications*, ser. Lecture Notes in Statistics. Springer New York, 2008, vol. 191, pp. 1–30.

[31] T. Nakagawa and S. Osaki, "The Discrete Weibull Distribution," *IEEE Trans. on Reliability*, vol. R-24, no. 5, pp. 300–301, Dec. 1975.

[32] T. Schon, F. Gustafsson, and P.-J. Nordlund, "Marginalized particle filters for mixed linear nonlinear state-space models," *IEEE Trans. on Signal Processing*, vol. 53, pp. 2279–2289, 2005.

[33] K. C. Mcgill, K. L. Cummins, and L. J. Dorfman, "Automatic decomposition of the clinical electromyogram," *IEEE Trans. on biomedical engineering*, vol. 32, no. 7, 1985.

[34] C. Katsis, Y. Goletsis, A. Likas, D. Fotiadis, and I. Sarmas, "A novel method for automated EMG decomposition and MUAP classification," *Artificial Intelligence in Medicine*, vol. 37, pp. 55–64, 2006.

[35] L. Ljung and T. Söderström, *Theory and Practice of Recursive Identification*. Massachusetts and London: The MIT Press, 1983.

[36] Q. Xia, M. Rao, Y. Ying, and X. Shen, "Adaptive fading kalman filter with an application," *Automatica*, vol. 30, no. 8, pp. 1333–1338, 1994.

[37] K. McGill, Z. Lateva, and H. Marateb, "EMGLAB: An interactive EMG decomposition program," *J. of Neuroscience Methods*, vol. 149, no. 2, pp. 121–133, 2005.

[38] D. Farina, R. Colombo, R. Merletti, and H. B. Olsen, "Evaluation of intra-muscular EMG signal decomposition algorithms," *J. of Electromyography and Kinesiology*, vol. 11, pp. 175–187, 2001.

[39] K. Kulasekera, "Approximate mles of the parameters of a discrete weibull distribution with type-i censored data," *Microelectronics Reliability*, vol. 34, no. 7, pp. 1185–1188, 1994.

[40] S. Yi, D. Wierstra, T. Schaul, and J. Schmidhuber, "Stochastic search using the natural gradient," in *In Proc. of the 26th Ann. Int. Conf on Machine Learning*, 2009, pp. 1161–1168.